Ultra-low icing adhesion of superhydrophobic coating based on synergistic effect of soft and stiffness particles

Houde Cheng[1], Guiyan Yang[1], Dan Li[1], Mengru Li[1], Yang Cao[1]*, Qiang Fu[2], Youyi Sun[1*]

1.School of materials science and Engineering, North University of China, Taiyuan 030051, P.R. China.

2.School of Civil and Environmental Engineering, University of Technology Sydney, Ultimo NSW 2007, Australia.

Abstract: A novel superhydrophobic coating composed of soft polydimethylsiloxane microspheres and stiffness SiO_2 nanoparticles was developed and prepared. This superhydrophobic coating did not only show excellent superhydrophobicity with a large water contact angle of 171.3°, but also exhibited good anti-icing performance and ultralow icing adhesion of 1.5k3Pa. Furthermore, the superhydrophobic coating displayed good icing/deicing cycle stability, in which the icing adhesion was still less than 10.0kPa after 25 cycles. This excellent comprehensive performance is attributed to stress-localization between ice and coating surface, resulting from the synergistic effect of soft and stiffness particles.. The work thus opens a new avenue to simultaneously optimize the anti-icing and icephobic performance of superhydrophobic surface for various applications.

Keywords: superhydrophobic surface, double-layer structure, icing adhesion, soft and stiffness particles.

Responding author: Fax: 86-351-3559669

E-mail address: syyi@pku.edu.cn (YY Sun), 121449463@qq.com (Y Cao)

1.Introduction

In a cold environment, ice is formed mainly through freezing rain, snow and frost[1-2]. In case of rain, snow or wet weather, ice may accumulate on the wings when an airplane during take off [3-4].The accumulation of ice is imperceptibly bringing many safety hazards to transportation [5], aerospace [6], maritime work and power transportation [7]. Therefore, anti-icing and/or icephobic technologies have been developed to prevent ice accumulation and reduce the safety hazards, such as active lipophobicity [8-9] or passive icephobicity [10-11]. Unfortunately, active lipophobicity (eg. electrothermal devices [12] and chemicals [13], or other physical methods[14]) shows labor-intensive, high cost and slow results [15], restricting its practical applications. So, the passive icephobicity is a promising method to prevent ice accumulation and reduce the safety hazards, in which special surface is designed to reduce ice adhesion [16]. When the ice adhesion on surface is enough small, the ice accretion is easily removed from surface by natural forces, such as wind, vibration or centrifugal force[17]. Recently, three kind of surfaces have been developed to reduce ice adhesion, including the superhydrophobic surfaces [18-19], slippery liquid-infused porous surface [20-21] and hydrated or non-freezing surfaces [22-23]. For superhydrophobic surfaces, the reducing ice adhesion was attributed to small contact area of ice droplets on the superhydrophobic surface, resulting from large water contact angle [24]. However, a high roughness is usually required to obtain large water contact angle for superhydrophobic surfaces, which easily leads to an increase of ice adhesion strength (even in the range of 100-500 kPa). Furthermore, during multiple icing/deicing cycles, the droplets will remain in the high roughness structure, further enhancing ice adhesion. These problems restrict the practical application of superhydrophobic surfaces in the field of anti-icing and icephobic technology[25-26]. For the slippery liquid infused porous surfaces (SLIPS), the reducing ice adhesion is attributed to the smooth nature of liquid surface with an adhesion strength ranging from 10 to 150kPa [27]. However, after several icing/deicing cycles, the liquid layer depletes and the ice adhesion increases to the order of 200 kPa [25]. For hydrated or non-freezing surfaces, the reducing ice adhesion is attributed to the lubricating film, resulting from water at freezing temperatures [28-29]. At higher than -25.0℃, the ice adhesion strength on the surface is in the range of 20-60 kPa [25]. However, at lower temperatures than -25.0℃, the change in molecular configuration of the transition film would drastically enhance the ice adhesion to more than 1000kPa [30]. From

above respects, it is still an ambitious challenge to develop a practical technology to reduce ice adhesion and prevent ice accumulation.

In this study, we reported a novel superhydrophobic coating to reduce ice adhesion and prevent ice accumulation. The superhydrophobic coating was constructed by combining PDMS soft particles with OTS@SiO_2 nanoparticles. The resulting surface had a unique micro-nano structure, low surface energy and excellent superhydrophobicity. In addition, ultra-low ice adhesion was also observed due to stress-localization, resulting from the synergistic effect of the soft and stiffness particles. When a weak force is applied, cracks are formed at the interface, and ice accretion is easily removed.

2. Experiment sections

2.1 Material

Dimethylsiloxane (BD-681) was purchased from Hangzhou Baoerde New Material Technology Co., Ltd. T-octylphenoxypolyethoxyethanol (Triton X-100) and triethoxyoctylsilane (OTS) were purchased from Aladdin. Tween 20 was purchased from Macklin. Anhydrous ethanol was purchased from Tianjin Damao. SiO_2 nanopartciles (45.0nm) was purchased from Macklin. Fluorocarbon resin was provided by Shanxi Dongfanghong Coating Co., Ltd. All reagents were used according to the instructions and no further purification is required.

2.2 Synthesis of Polydimethylsiloxane (PDMS) microspheres

PDMS microspheres are synthsized by emulsion polymerization method as shown in following. 0.75ml T-octylphenoxypolyethoxyethanol (OPE) and 50 mL water were mixed under ultrasonication for 5.0min. 4.0g Dimethylsiloxane and 4.0g curing agents (BD-681 B) were mixed under magnetic stirring for 5.0min, and then placed in vacuum oven for 30.0min at room temperature. Then, the OPE/water mixing solution was slowly added to the Dimethylsiloxane/curing agents mixing solution under mechanically stirring at a speed of 2000 rpm for 1.0h. Above mixture was reacted at 80℃ for 1.0h under mechanically stirring, forming PDMS microspheres. Then, the PDMS microsphere dispersion solution was filtered with a 600-mesh stainless steel mesh to remove large microspheres. The PDMS microsphere dispersion solution was centrifuged at 3000 rpm for 15.0min and then washed with water and ethanol for three times. The pure PDMS microspheres were further dispersed in ethanol containing with 0.1wt% Tween 20, forming stable PDMS microsphere dispersion ethanol (16.5wt%)..

2.3 Preparation of superhydrophobic coating based on soft and stiffness particles

The superhydrophobic coating was prepared by a three-step method. Firstly, OTS modified SiO_2 nanoparticles (OTS@SiO_2) were prepared according to our previous work [31]. Then, 0.4 g OTS@SiO_2 nanoparticles were added to 10 mL PDMS microspheres dispersion ethanol (16.5wt%) under ultrasonic stirring for 5.0 min. Secondly, 5.0 g fluorocarbon resin (FEVE) paints and 1.0 g curing agent were fully mixed, and evenly scraped on the surface of glass substrate. The FEVE coating was pre-cured at 80.0℃ to afford a semi-dry structure. Finally, the mixture of OTS@SiO_2 and PDMS microsphere dispersion ethanol was uniformly sprayed on the surface of semi-dry FEVE coating, and the double-layer coating was further cured at 80.0℃ for 12.0h. In a comparison, single OTS@SiO_2 nanoparticles or PDMS microspheres were directly coated on the FEVE coating.

2.4 Characterization

The micro-structure of particles and coating was measured by scanning electron microscope (SEM, Su-8010).

A 3D profile scanner (Super View W1) was used to characterize the surface roughness of coating.

The water contact angles (WCAs) were measured by contact angle tester (DSA100, Germany). In order to accurately determine the water contact angles, the average values were measured at three different places.

2.5 Anti-icing performance

Static anti-icing test was shown below. The prepared surface was placed in a low-temperature oil bath (temperature of -20.0℃, humidity 30%) for 5.0min to equilibrate with the ambient temperature. Then 9.0 μL of small water droplets were dropped on the surface. At the same time, temperature changes on the surface of the droplets were recorded using infrared thermal imaging and the change state of the water droplets was recorded by a CCD high-speed camera (CP70-1HS-M-1900, Optronis) with a camera speed of 1m/s and a resolution of 1280×860.

Dynamic anti-icing test was shown below. Three surfaces were placed in a low-temperature oil bath (temperature of -10℃, humidity 30% RH) with an inclination angle of 15.0° for 5.0min and the temperature was monitored by an infrared thermal imaging camera (FLUKE Ti400, accuracy ±2°C) with an actual temperature measurement range of -30~1200 and a resolution of 640×480. After reaching the equilibrium temperature, water droplets were dropped on the surface at a

constant speed, and the change of water droplets on the surface was recorded.

2.6 Characterization of icing adhesion

The ice adhesion test was shown below. First, a hollow cylinder with an inner diameter of 6.0mm was treated with low surface energy treatment, and then it was placed on the surface. The experimental setup was placed in an environment of -20.0℃/-25.0℃ and 30%/60% RH. 1.0 mL water was added to the cylinder and frozen for 50.0min. After freezing, 2.0 mL water was further added to above cylinder and frozen for 70 min. The frozen surface was placed under -20.0℃/-25.0℃ and 30%/60% RH, and then a digital push-pull gauge (N_{Max}=100N) was pushed slowly to test the adhesion of the ice on the surface.In this experiment, three samples.were used, in which icing adhesion of two different positions in each sample was tested. Then the average value was calculated from the six values. All temperatures were measured by infrared thermal imaging cameras.

3. Results and discussion

In order to prepare superhydrophobic coating with low icing adhesion, we proposed a due-layer structure consisting of a FEVE bottom layer and a top rough layer based on soft and stiffness particles. The bottom layer based on FEVE coating acts as adhesive agent of the PDMS microspheres and OTS@SiO_2 nanoparticles. The top layer based on assemble of PDMS microspheres and OTS@SiO_2 nanoparticles provide excellent superhydrophobicity and soft/stiff alternation structure. The micro-structure of superhydrophobic coating was firstly characterized by the SEM images as shown in Fig.1. We observed rough surfaces with micro- and/or nano-sized particles for all samples (in Fig.1A-C). Specifically, the top layers made of PDMS microspheres (*ca.* 4.5μm) or OTS@SiO_2 nanoparticles (*ca.* 4.5μm) showed a high or relatively low roughness, respectively (Fig.1D-E). For PDMS/SiO_2 hybrid coating, we observed both large PDMS microspheres and small OTS@SiO_2 nanoparticles, where the nanoparticles filled in the gaps between microspheres (Fig.1E). Of particular note, both the OTS@SiO_2 nanoparticles and PDMS microspheres were tightly embedded in the FEVE coating. These results confirmed the successfully formation of superhydrophobic surface based on assemble of PDMS microspheres and OTS@SiO_2 nanoparticles.

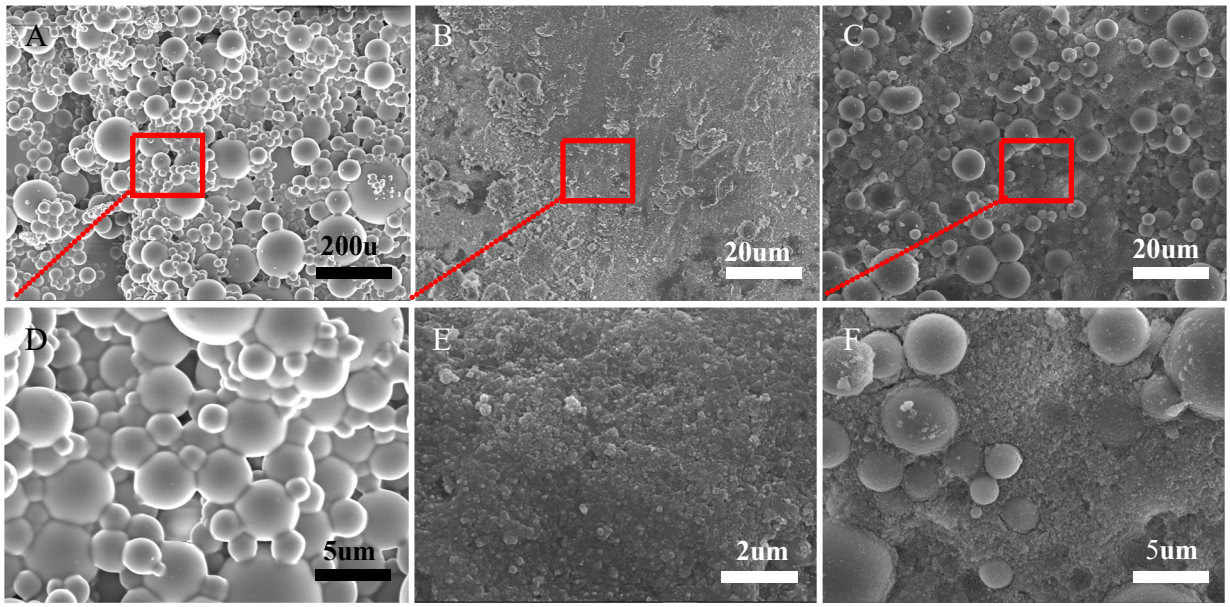

Fig.1. SEM images of (A, D) PDMS based surface, (B, E) OTS@SiO_2 based surface and (C, F) PDMS/SiO_2 based surface.

The surface roughness of all coatings was characterized by the noncontact white light profilometer as shown in Fig.2A-C. It showed a relatively large surface roughness (Sa=1.067μm) for the PDMS microsphere-based surface (Fig.2A). In the case of OTS@SiO_2 nanoparticles-based surface, a relatively smooth surface with a low surface roughness of 0.265μm was observed (Fig.2B). A similar low surface roughness (Sa=0.277μm) was also observed for the PDMS/SiO_2 hybrid surface. As well-known, a low surface roughness is beneficial to reduce ice adhesion and anti-icing [24]. The superhydrophobicity of all coatings was further characterized and compared as shown in Fig.2D-F. It was observed that water drops could remain spherical structure on all surfaces, indicating the good hydrophobicity of these coatings. In a comparison, the PDMS/SiO_2 hybrid surface showed the largest WCA of 171.3° and smallest SA of 0° (Fig.2D). In order to better reflect the excellent superhydrophobicity, the bounce performance of water drop on the PDMS/SiO_2 surface was also characterized by CCD high-speed camera (in Video1, Supporting Information). When 9.0μL water was dropped onto the surface from a height of 5.0 cm, the water droplet shrinked, rebounded and then jumped out of the surface through constant rebound. This result indicated that the water droplet was completely non-adhesive on the surface. Compared to the hybrid surface, the PDMS and

OTS@SiO_2 based surfaces showed smaller WCAs of 150.3° and 162.8°, (Fig.2E and Fig.2F) and larger SAs of 5.0° and 2.0°, respectively. The result was attributed to a greater roughness of PDMS based surface comparing to the PDMS/SiO_2 and SiO_2 based surface. The OTS@SiO_2 with lower surface energy (1.4mN/m) was also key role for above result comparing to that (11.0mN/m) of pure PDMS [31-32]. Although the PDMS/SiO_2 based surface had a similar roughness with the SiO_2 based surface, yet it showed a larger WCA and a smaller SA. The result could be attributed to a synergistic effect of soft PDMS microspheres and stiffness OTS@SiO_2 nanoparticles. These results further reveal that the prepared hybrid surface has excellent superhydrophobicity and low surface roughness, which are important for improving the anti-icing and icephobic properties.

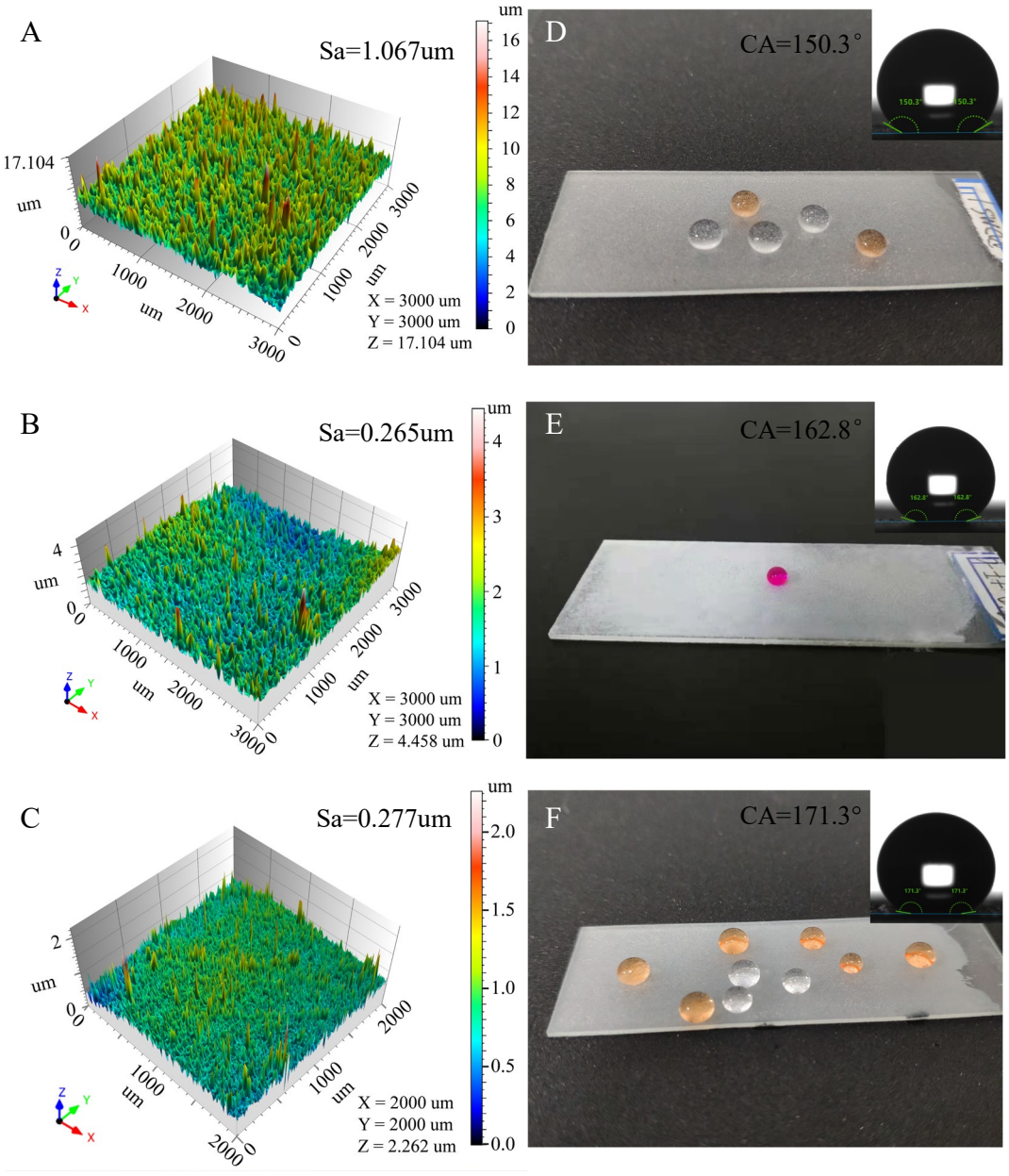

Fig.2. 3D profile scanning analysis of (A) PDMS, (B) SiO_2 and (C) PDMS/SiO_2 based surfaces. Optical photos of water droplets on various surfaces made of (D) PDMS microspheres, (E) OTS@SiO_2 nanoparticles and (F) PDMS/SiO_2 mixture. The insets correspond to the optical photos of WCA.

The anti-icing performance of all coatings was evaluated by a high speed video equipment as shown in Fig.3A. When the water droplet was dropped onto the PDMS/SiO_2 based surface (WCA=171.3°) from a height of 10.0cm, it rapidly rolled down at a cold temperatures of -10.0°C and an inclination angle of 15.0° (Fig.3A-b). In contrast, the water droplets adhered on the surfaces of PDMS based and SiO_2 based coatings under the same condition (Fig.3A-a and c, respectively). These results indicated that the PDMS/SiO_2 based surface displayed a strong anti-icing ability at low temperature. The icing process of water droplets on these surfaces was further characterized and compared by a high-speed camera as shown in Fig. 3B. The opaque ice crystals grown from bottom to the top [33]. In addition, it clearly showed various froze times of water droplet for various surfaces. For the PDMS/SiO_2 based surface, the water droplet showed a turbid state at 150.0s, indicating formation of ice nucleation. After 316.0s, the water droplet completely froze and the tip appeared on the surface as shown in Fig.3B-b. In a comparison, the icing time was reduced to 207.0s and 239.0s for the single PDMS and SiO_2 based surface, respectively. These results revealed that the good anti-icing ability of PDMS/SiO_2 based surface was attributed to prolong the froze time, strongly depending on the WCA and sliding angle.

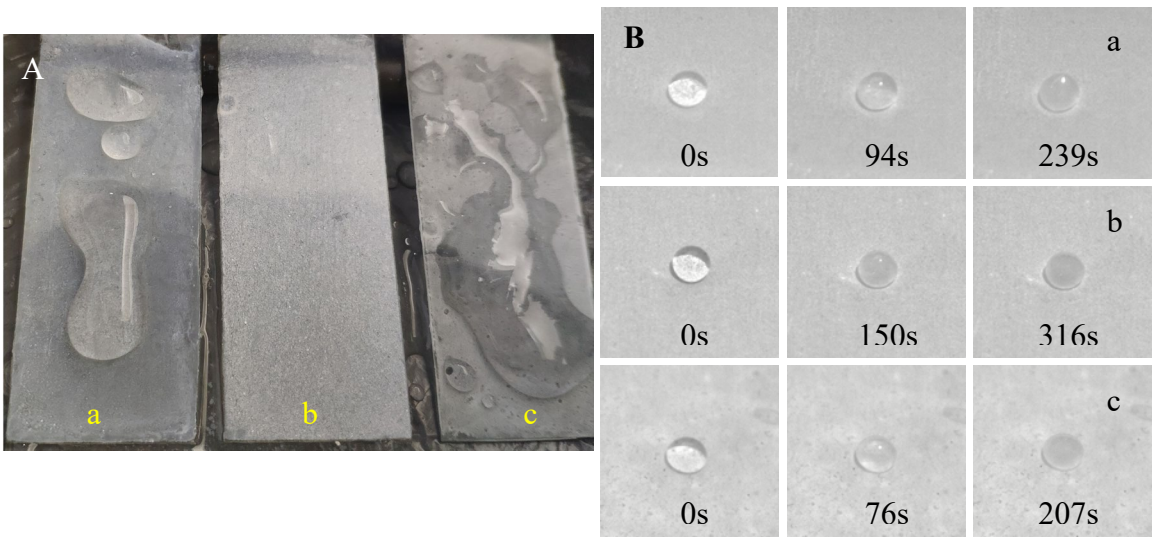

Fig.3. (A) Dynamic and (B) Static anti-icing optical photographs of various surfaces based on (a) SiO_2, (b) PDMS/SiO_2 and (c) PDMS at -10.0°C.

The icing process on different surfaces was further recorded by thermal infrared imaging equipment as shown in Fig.4. Fig.4A showed the thermal infrared images of water droplets on different surfaces at -20.0°C as function of time. Although the temperature was below 0°, yet the water droplets did not freeze, suggesting the formation of supercooled water. As expected, the temperature of the water droplets gradually decreased with increasing in exposure time. It cooled down to -1.6°C, -2.1°C and -15.5°C at same cooling time of 88.0s for various surfaces based on PDMS/SiO_2, SiO_2 and PDMS, respectively. These results confirmed that the PDMS/SiO_2 based surface could effectively reduce heat transfer rate between water droplet and surface, prolong cooling time of water. The transient temperature profiles of water droplets on surface as function of cooling time were also concluded in Fig.4B. The subcooling equilibrium temperatures are ca. -1.6°C, -1.8°C and -2.3°C for the surfaces based on PDMS/SiO_2, SiO_2 and PDMS, respectively, the temperature curve shows that the PDMS/SiO_2 surface has a longer subcooling equilibrium time (120s), which is 1.5 times and 3 times higher than that of the SiO_2 and PDMS surfaces, respectively. The higher equilibrium temperature of PDMS/SiO_2 based surface was attributed to smaller heat transfer rate, resulting from the smaller contact area between the water droplet and the surface with larger CA. The water droplet on surface slightly cooled down, and prolonged time to trigger the ice nucleation.These results further suggested that the good anti-ability of PDMS/SiO_2 based surface was attributed to its low heat transfer rate, delaying the formation of ice nucleation.

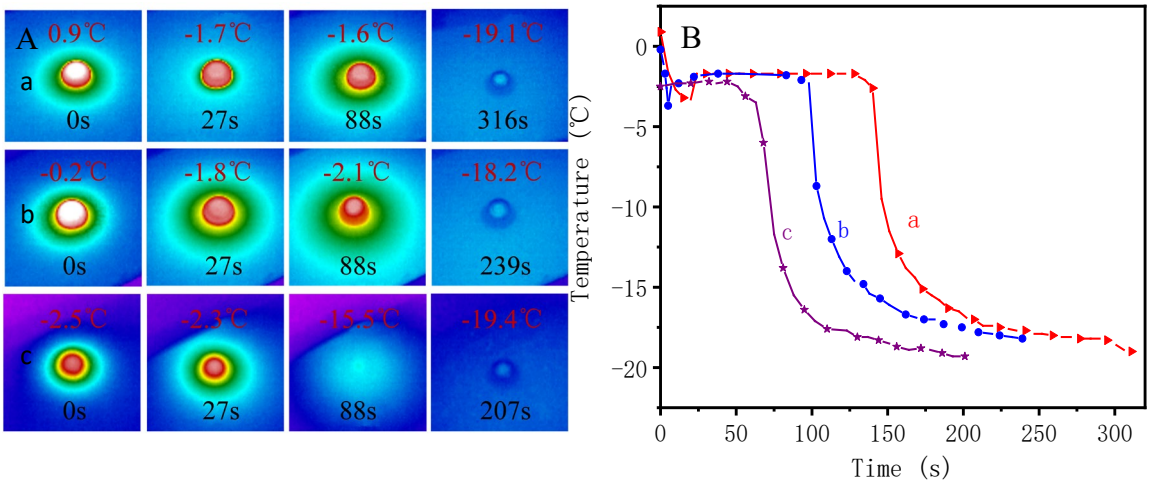

Fig.4. (A) IR images and (B) transient temperature profiles of water droplets on (a) PDMS/SiO_2, (b) SiO_2 and (c) PDMS based surfaces at -20°C.

The adhesion strength of ice crystals on different surfaces was characterized by using a self-made setup (Fig.5A). A shear force (F) was applied to detach ice, which was determined by force sensor. The ice adhesion strength (G) at the interface can be written as Eq 1 [34]:

$$G=F/\sigma_s \quad (1)$$

Where F is the push-pull force, σ_s is the contact area between the ice and the surface. Here, the F was obtained by average of six values. The averaged ice adhesion strength is concluded in Fig.5B and Fig.5C. We found that the PDMS and SiO_2 based surfaces displayed relatively high ice adhesion strength of 48.3kPa and 27.3kPa at -20.0℃ and 30% RH, respectively. Surprisingly, the PDMS/SiO_2 based surface showed ultra-low ice adhesion strength of ca. 1.53 kPa, which is 32 or 18 times lower than that of PDMS and SiO_2 based surfaces in the same environment. In the same environment with -25.0℃ and 60% RH, it showed similar results. The ice adhesion strength of PDMS/SiO_2, PDMS and SiO_2 based surfaces showed 6.5 kPa, 55.5kPa and 32.4kPa, respectively. Especially, the ice adhesion strength (6.5 kPa) of PDMS/SiO_2 based surfaces still showed far lower ice adhesion strength than 20.0kPa at low temperature (-25.0℃) and high humidity (60%) for practical application. The ice adhesion strength of PDMS/SiO_2-based surface was also compared with that of other surfaces reported in previous works as shown in Fig.5C [10, 34-49]. It clearly showed lowest ice adhesion strength so far among all the reported data. These results confirmed the formation of superhydrophobic surface with ultra-low ice adhesion.

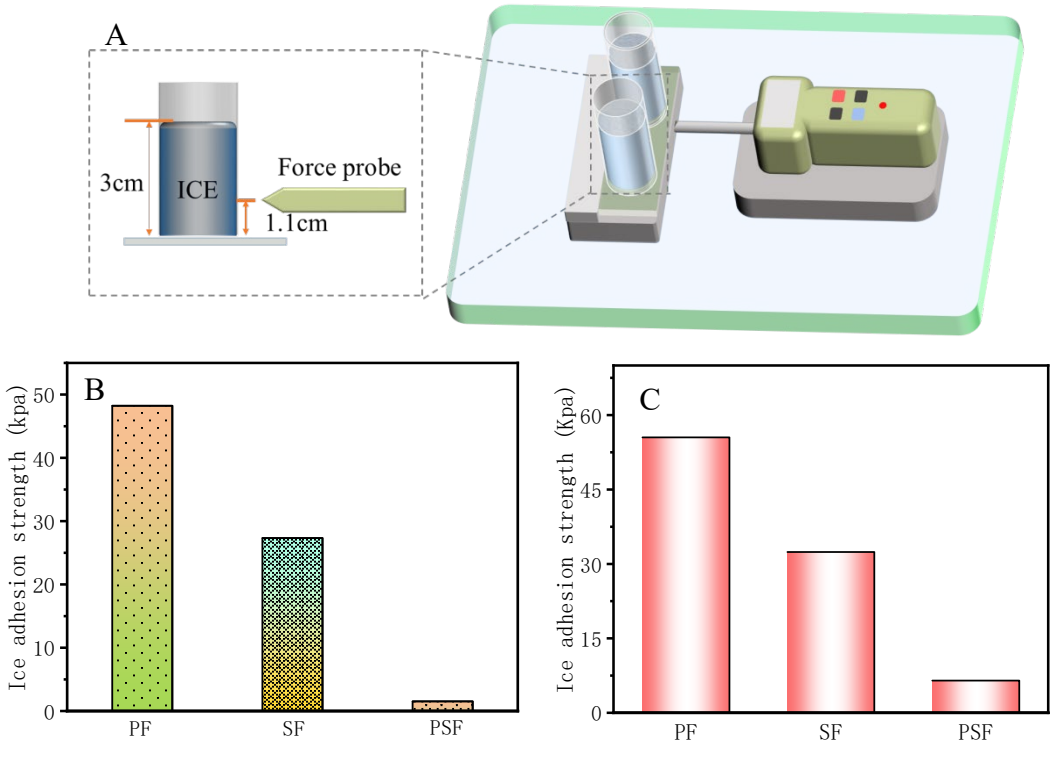

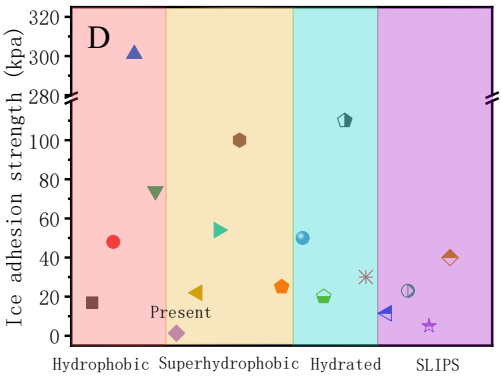

Fig.5. (A) Schematic illustration of the ice detachment process from the icephobic material.Adhesion strength of ice on PDMS (PF), SiO_2 (SF) and PDMS/SiO_2 (PSF) based surface (B) at -20℃, 30% RH and (C) at -25℃, 60% RH.(D) Comparison of ice adhesion strength of PDMS/SiO_2 based surface with other anti-icing surfaces.

As well-known, when the ice adhesion force is lower than 20KPa, the ice can fall off on their own under the action of breeze, slight vibration or gravity [17]. Here, the self-deicing ability of present PDMS/SiO_2 based surface was also evaluated and compared at ~4.0±1.0℃ as shown in Fig.6. It needed 105.0s for the ice cube slipping from PDMS/SiO_2 based surface under gravity as shown in Fig.6B. In a comparison, the ice cubes began to slip from PDMS and SiO_2 based surface at 159.0s and 132.0s, respectively (in Fig.6C-D). These results confirmed the good self-deicing ability of present superhydrophobic surface, especially for PDMS/SiO_2 based surface due to ultra-low ice adhesive strength.

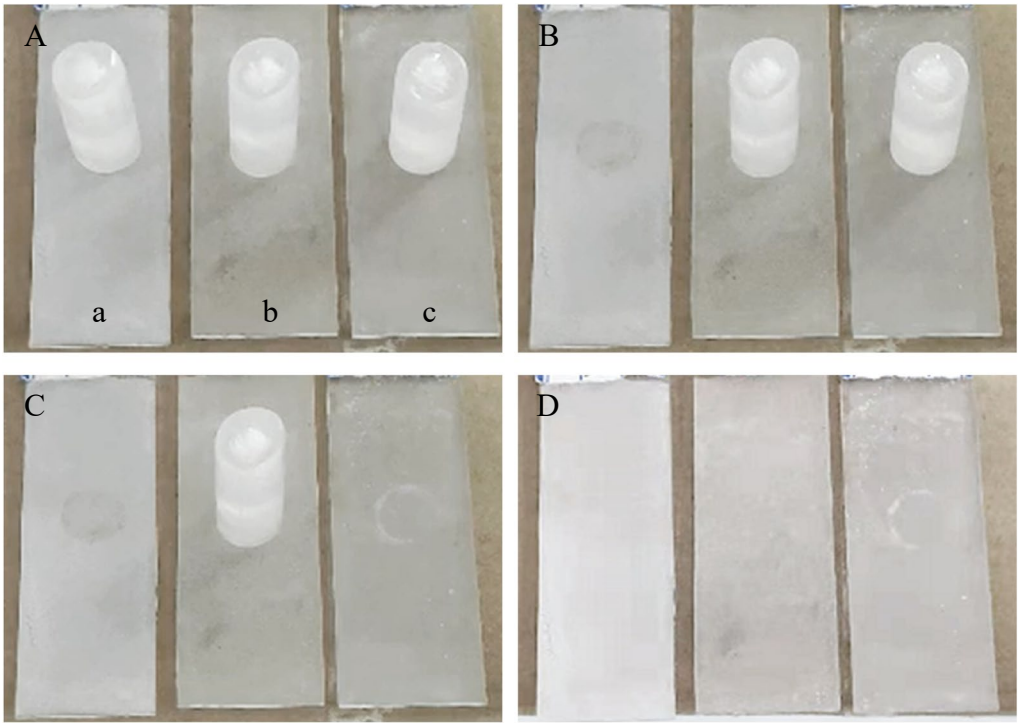

Fig.6. Optical photos of ice cubes on (a) PDMS/SiO_2, (b) SiO_2 and (c) PDMS based surfaces after different time intervals, (A) 0s, (B)105.0s, (C) 132.0s and (D) 159.0s.

The mechanical stability of PDMS/SiO_2 based surface was also evaluated by mechanical abrasion test as shown in Fig.7A-C. The superhydrophobic surface was put on 400-Mesh sandpaper under 200.0g weight (Fig.7A). Then the sample was evenly pushed back and forth for 10.0 cm, which was defined as one abrasion cycle. As shown in inset of Fig.1A and Video 2 (Supporting Information), after 100 abrasion cycles the PDMS/SiO_2 based surface still maintained its superhydrophobicity (CA=168.0°) and displayed a small SA of 0°. As shown in Fig.7B, the micro-structure of PDMS/SiO_2 based surface after 100 abrasion cycles was further characterized as shown in Fig.7B. The large PDMS microspheres were worn by mechanical abrasion, forming relatively smooth surface. However, the ice adhesive strength of the PDMS/SiO_2 based surface slightly increased after 100 abrasion cycles, but it still showed low ice adhesive strength of ca 7.0KPa (Fig.7C).Above results were difficult to be observed in previous works[39, 50], in which the low-ice adhesion surfaces was destroyed after a period of mechanical abrasion, resulting in a sharp increase in ice adhesion strength. The different result was attributed to that the surface still maintained soft/stiffness alternation structure (inset of Fig.7C) and good superhydrophobicity (CA=168.0°). In addition, smooth surface was also benefit to reduce ice adhesive strength by 100 abrasion cycles (inset of Fig.7C)[24]. The icing/deicing durability of the PDMS/SiO_2 based surface was further evaluated as shown in . After 25 cycles, some PDMS microspheres on surface were removed by icing/de-icing test, yet it still maintained high surface roughness as shown in Fig.7D. It was found that the hydrophobicity (CA=144.0°) of PDMS/SiO_2 based surface was obviously reduced. Although the ice adhesion strength of surface increased from 1.5kPa to 9.0kPa (Fig. 7E), yet it still showed far lower ice adhesion strength than 20.0kPa for practical application. These results further indicated the excellent mechanical stability and high icing/deicing durability of the PDMS/SiO_2 based surface.

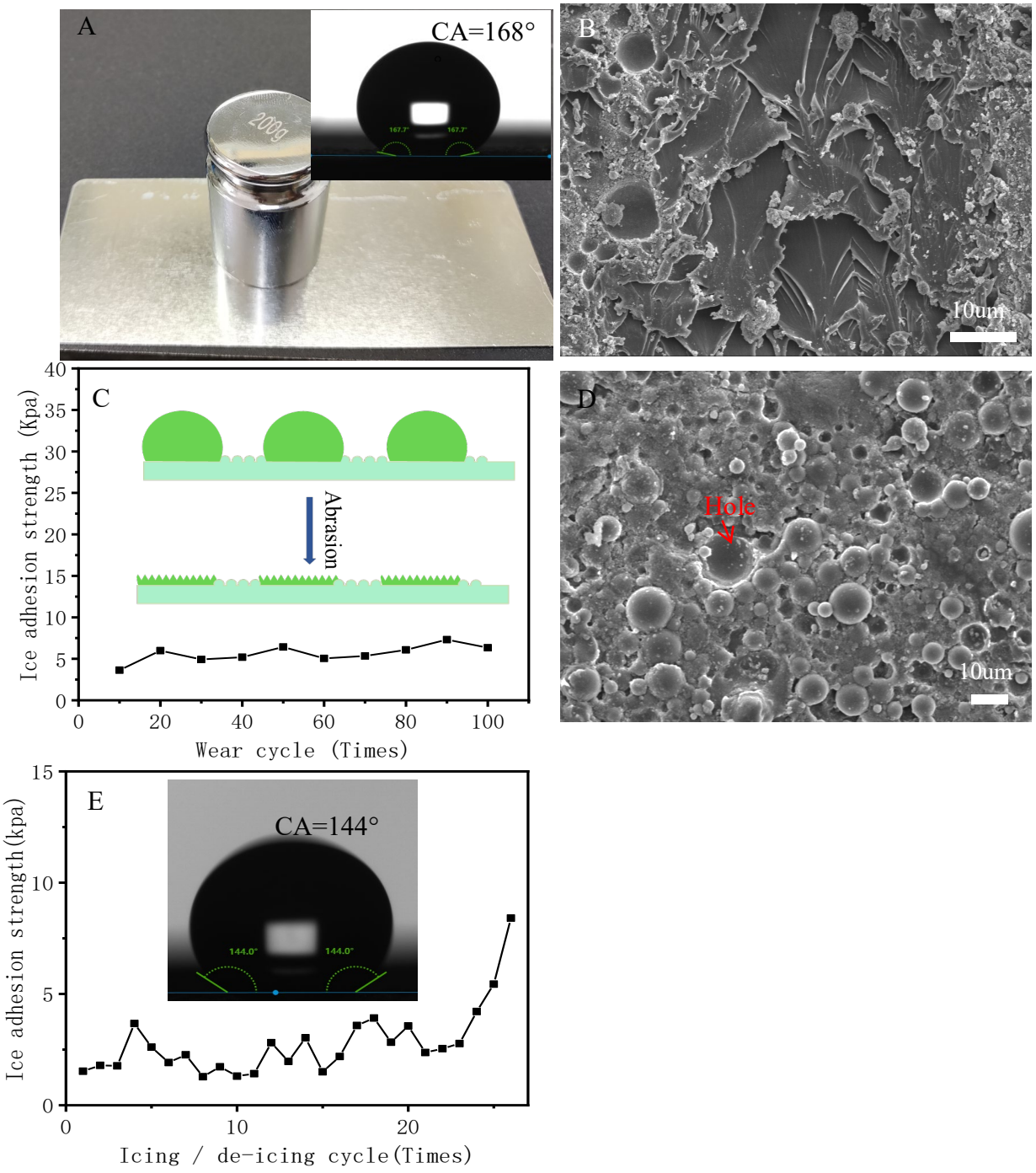

Fig.7. (A)Optical photo of the sandpaper abrasion test. (B) SEM image of PDMS/SiO_2 based surface after 100 abrasion cycles. (C) Ice adhesive strength of PDMS/SiO_2-based surface as a function of abrasion cycles. (D) SEM image of the surface after 25 icing/de-icing cycles (E) Ice adhesive strength of PDMS/SiO_2-based surface as a function of icing/de-icing cycles.The insets of A and B are the WCA and Schematic illustration of surface after 100 abrasion cycles, respectively. The inset of E is the WCA of surface after 25 icing/de-icing cycles.

A new experiment was developed to investigate the anti-icing mechanism of the PDMS/SiO_2 based surface with ultra-low ice adhesive strength. As shown in Fig. 8A, a large PDMS sphere containing RhB was synthesized and embedded in FEVE

coating by the template method. Fig. 8A(a-b) showed the top and side optical photos of the PDMS sphere in water, respectively. We observed a hemisphere with pink color, and the PDMS hemispheres were surrounded by water. When the water was changed to ice at a temperature of -20.0°C and a humidity of 30%RH, it was found that the ice caused the PDMS hemisphere to squeeze in all directions, and the sphere was severely deformed as shown in Fig.8A(c-d). The deformation of PDMS microspheres would produce a opposite force on the ice cube, while there was no force between hard OTS@SiO_2 nanoaprticles and ice cube. The nonuniform force is defined as stress-localization as shown in Fig. 8B. When an external force is applied to ice cube, cracks are easily formed between ice cube and PDMS microsphere due to the perpendicular stress-localization, resulting in ultra-low ice adhesion strength. From above respects, we can conclude that the synergistic effect of the soft and stiffness spheres plays a key role for the formation of stress-localization and ultra-low ice adhesion strength.

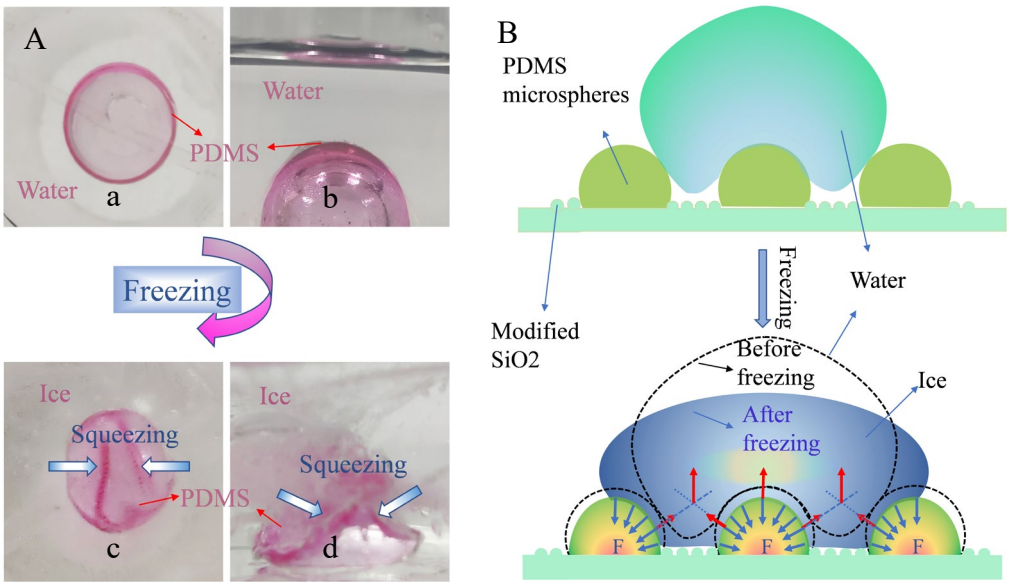

Fig.8. (A)Optical photos of PDMS sphere embedded in FEVE coating: (a, c) top- and (b, d) side-view images. (B) The proposed mechanism diagram of PDMS/OTS@SiO_2-based superhydrophobic surface with ultra-low ice adhesion.

To further confirm above synergistic effect, ice adhesive strength of PDMS/SiO_2 based surface was also characterized as function of modulus of PDMS microspheres.The modulus of PDMS microspheres was adjusted by introducing rGO into PDMS microsphere as shown in Fig.9. It clearly showed that the modulus of PDMS increased with increasing in content of rGO. Specifically, the modulus of

pristine PDMS and PDMS/rGO composite (1.0 wt%) was ca. 0.09 MPa and 0.27 MPa, respectively. The PDMS/rGO composite microspheres were then used to construct superhydrophobic surfaces. The ice adhesion strength of the superhydrophobic surfaces was also characterized as a function of rGO contents as showed in Fig.9B. As expected, the ice adhesion strength of the superhydrophobic surface increased with increasing in contents of rGO. The PDMS/SiO_2 based surface without rGO showed the lowest ice adhesion strength of 1.53kPa. In contrast, the superhydrophobic surface with 1.0wt% rGO displayed an enhanced ice adhesion strength of 7.7KPa. This result further confirmed that the synergetic effect of the soft and stiffness spheres leaded to a stress-localization effect, resulting in ultra-low ice adhesion force.

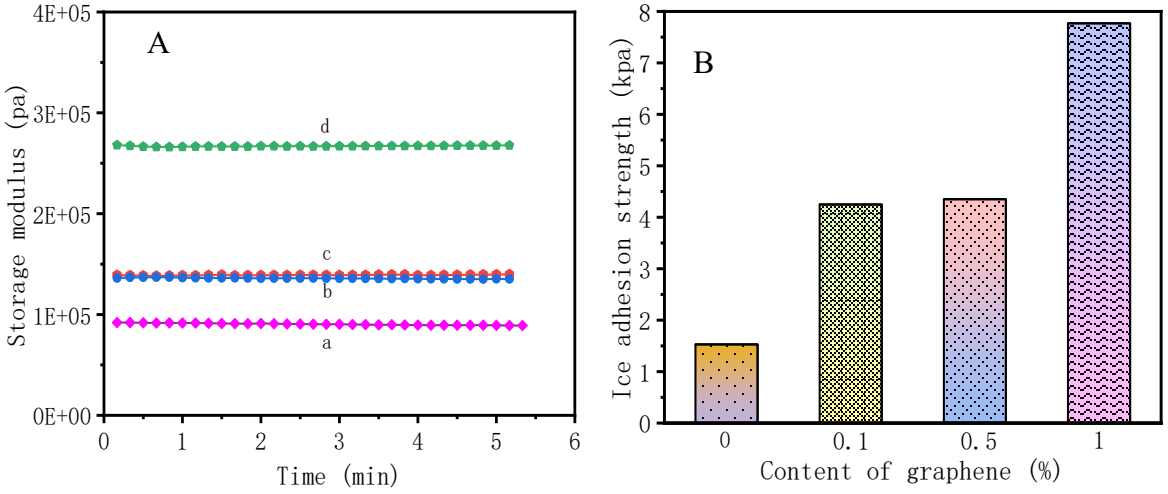

Fig.9. (A) Dynamic shear modulus of PDMS/rGO composites with different rGO contents: (a) 0wt%, (b) 0.5wt%, (c) 0.1wt% and (d) 1.0wt%. (B) The ice adhesion of PDMS/OTS@SiO_2 based surface as a function of rGO contents.

The ice adhesion energy between ice and the surface was determined by Molecular dynamics simulation. The length and width of the constructed model are both 50.0Å, and the side length of the ice block is 27.1Å. Then, AC was used to construct a PDMS substrate with a density of 0.985g mL^{-1}. Finally, the IH structure of the ice and the base are formed into a two-layer model by layer building, and then the dynamic equilibrium is performed at a temperature of 253k, a compass force field and a NVT ensemble of 200 ps. Fig.10 shows the molecular electrostatic potential (MEP) of ice/PDMS, ice/OTS@SiO_2 and ice/FEVE. Furthermore, the interaction energy (E_{ab}, or adhesion strength) between ice and materials is calculated according to following

Eq (2)[51].

$$E_{ab} = E_{Total} - E_a - E_b \quad (2)$$

Where the E_{ab}, E_{Total}, E_a and E_b are interaction energy between ice and surface, energy of the whole model, energy of ice cubes and materials surface energy, respectively. The interaction energy (E_{ab}) of ice/PDMS, ice/OTS@SiO_2 and ice/FEVE is *ca.* 5018.5kcal/mol, -62200.4kcal/mol and 5633.8kcal/mol, respectively. Surprisingly, the E_{ab} of ice/FEVE is the largest, which is inconsistent with the experimental results. The interaction of ice and PDMS/OTS@SiO_2 based surface was smaller than that of OTS@SiO_2 or PDMS based surfaces. This result thus indicated that the ultra-low ice adhesion of PDMS/OTS@SiO_2 based surface was not due to interaction energy between the ice and the surface.

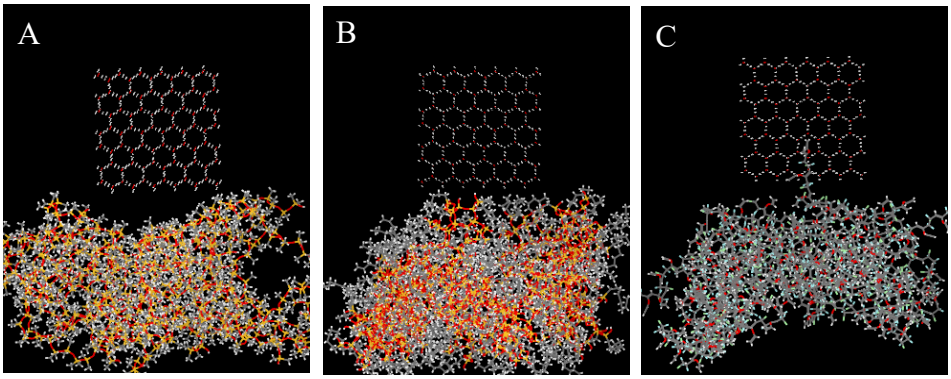

Fig.10. Interaction kinetic calculation of the interaction energy of (A) ice/PDMS, (B) ice/OTS@SiO_2 and (C) ice/FEVE interfaces.

Table 1. Interaction energy between ice and different surfaces.

Samples	Total energy (kcal/mol)	Energy (ice) (kcal/mol)	Energy (basement) (kcal/mol)	E_{ab} (kcal/mol)
PDMS	-44880.6	0	-49899.0	5018.5
OTS@SiO_2	-48275.1	0	13925.3	-62200.4
FEVE	13628.9	0	7995.1	5633.8

Combining the experimental with simulated results, the good anti-icing performance, ultra-low ice adhesion and good icing/deicing cycle stability of the PDMS/OTS@SiO_2 based surface are attributed to the following reasons. Firstly, the

PDMS/OTS@SiO_2 based surface has excellent superhydrophobicity, large WCA, low surface energy and low surface roughness .The large WCA leads to smaller contact area between water droplets and the surface, reducing the heat transfer rate between the cold surface and water droplets[31-32]. This also leads to a reduction in the contact area between the ice and the surface, thereby improving anti-icing performance and reducing ice adhesion. The lower surface energy results in smaller van der Waals forces between the ice and the surface, resulting in lower ice adhesion. The low surface roughness limits the penetration of water into the porous structure and the formation of mechanical interlock, thereby reducing ice adhesion. At the same time, the surface with low surface roughness has a good free-energy barrier for the formation of ice nucleation, thereby enhancing the anti-icing performance. In addition, the stiffness SiO_2 incorporated into the surface can also bring excellent mechanical stability. Of particular note, although the superhydrophobic surfaces reported in previous work [52-53] showed similar WCA, surface energy and surface roughness to the present surface, the ice adhesion of the present superhydrophobic surface is much lower than that of other superhydrophobic surfaces. Secondly, the synergistic effect of the soft and stiffness spheres leads to stress-localization, which plays a key role in ultra-low ice adhesion. When low modulus PDMS microspheres are introduced onto the anti-icing surface, the ice detached from PDMS microspheres, and a local cavity (i.e. crack) is formed between the ice and the PDMS microspheres with minimal force. Such local cracks will generate elastic stress fields around the cracks. This induced shear stress field opens the crack front and causes crack growth and fracture at the interface.

4. Conclusion

In summary, a novel superhydrophobic surface based on the assembly of soft and stiffness particles was developed and prepared. The superhydrophobic surface shows excellent anti-icing performance, icephobic performance with ultra-low icing adhesion, self-deicing ability and good icing/deicing cycle stability. These results are attributed to the excellent superhydrophobicity and stress-localization, resulting from the synergistic effect of soft microsphere and stiffness nanoparticles. Furthermore, after 100 mechanical abrasion cycles, the superhydrophobic surface can still maintain low ice adhesion and superhydrophobicity, which is rarely reported in previous literature. This work thus opens a new avenue to develop anti-icing and icephobic coasting/surface for various practical applications.

Acknowledgment

The authors are grateful for the support of the National Natural Science Foundation of China under grants (51773184 and U1810114), Shanxi Provincial Natural Science Foundation of China (201803D421081 and 201801D121104).

References

[1] Wang G, Guo Z. Liquid infused surfaces with anti-icing properties[J]. Nanoscale, 2019, 11(47): 22615-22635.

[2] Pan, R.; Zhang, H.; Zhong, M., Triple-Scale Superhydrophobic Surface with Excellent Anti-Icing and Icephobic Performance via Ultrafast Laser Hybrid Fabrication. ACS Applied Materials & Interfaces 2021, 13 (1), 1743-1753

[3] Zhang X, Wu X, Min J. Aircraft icing model considering both rime ice property variability and runback water effect[J]. International Journal of Heat and Mass Transfer, 2017, 104: 510-516.

[4] Tarquini S, Antonini C, Amirfazli A, et al. Investigation of ice shedding properties of superhydrophobic coatings on helicopter blades[J]. Cold regions science and technology, 2014, 100: 50-58.

[5] Tan T, Xing C, Tan Y, et al. Safety aspects on icy asphalt pavement in cold region through field investigations. Cold regions science and technology, 2019, 161: 21-31.

[6] Sujata M, Madan M, Raghavendra K, et al. Unraveling the cause of an aircraft accident. Engineering failure analysis, 2019, 97: 740-758.

[7] Cerrai D, Koukoula M, Watson P, et al. Outage prediction models for snow and ice storms. Sustainable Energy, Grids and Networks, 2020, 21: 100294.

[8] Wang, F.; Tay, T. E.; Sun, Y.; Liang, W.; Yang, B., Low-voltage and -surface energy SWCNT/poly(dimethylsiloxane) (PDMS) nanocomposite film: Surface wettability for passive anti-icing and surface-skin heating for active deicing. Composites Science and Technology 2019, 184, 107872.

[9] Ibrahim, Y.; Kempers, R.; Amirfazli, A., 3D printed electro-thermal anti- or de-icing system for composite panels. Cold Regions Science and Technology 2019, 166, 102844.

[10] Dou R, Chen J, Zhang Y, et al. Anti-icing coating with an aqueous lubricating

layer[J]. ACS applied materials & interfaces, 2014, 6(10): 6998-7003.

[11] Li Y, Li B, Zhao X, et al. Totally waterborne, nonfluorinated, mechanically robust, and self-healing superhydrophobic coatings for actual anti-icing[J]. ACS applied materials & interfaces, 2018, 10(45): 39391-39399.

[12] Zhang, Z.; Chen, B.; Lu, C.; Wu, H.; Wu, H.; Jiang, S.; Chai, G., A novel thermo-mechanical anti-icing/de-icing system using bi-stable laminate composite structures with superhydrophobic surface. Composite Structures 2017, 180, 933-943.

[13] Ke, C.; Li, Z.; Liang, Y.; Tao, W.; Du, M., Impacts of chloride de-icing salt on bulk soils, fungi, and bacterial populations surrounding the plant rhizosphere. Applied Soil Ecology 2013, 72, 69-78.

[14] Wang, Y.; Xu, Y.; Huang, Q., Progress on ultrasonic guided waves de-icing techniques in improving aviation energy efficiency. Renewable and Sustainable Energy Reviews 2017, 79, 638-645.

[15] Fakorede, O.; Feger, Z.; Ibrahim, H.; Ilinca, A.; Perron, J.; Masson, C., Ice protection systems for wind turbines in cold climate: characteristics, comparisons and analysis. Renewable and Sustainable Energy Reviews 2016, 65, 662-675.

[16] Wang, T.; Zheng, Y.; Raji, A.-R. O.; Li, Y.; Sikkema, W. K. A.; Tour, J. M., Passive Anti-Icing and Active Deicing Films. ACS Applied Materials & Interfaces 2016, 8 (22), 14169-14173.

[17] Golovin, K.; Dhyani, A.; Thouless, M. D.; Tuteja, A., Low–interfacial toughness materials for effective large-scale deicing. Science 2019, 364 (6438), 371-375.

[18] Wu, B.; Cui, X.; Jiang, H.; Wu, N.; Peng, C.; Hu, Z.; Liang, X.; Yan, Y.; Huang, J.; Li, D., A superhydrophobic coating harvesting mechanical robustness, passive anti-icing and active de-icing performances. Journal of Colloid and Interface Science 2021, 590, 301-310.

[19] Tan, X. Y.; Wang, Y.; Huang, Z. T.; Sabin, S.; Xiao, T.; Jiang, L. H.; Chen, X. B., Facile Fabrication of a Mechanical, Chemical, Thermal, and Long-Term Outdoor Durable Fluorine-Free Superhydrophobic Coating. Advanced Materials Interfaces 2021, 2002209, 1-10.

[20] Cai, G.; Liu, F.; Wu, T., Slippery liquid-infused porous surfaces with inclined

microstructures to enhance durable anti-biofouling performances. Colloids and Surfaces B: Biointerfaces 2021, 202, 111667.

[21] Sett, S.; Oh, J.; Cha, H.; Veriotti, T.; Bruno, A.; Yan, X.; Barac, G.; Bolton, L. W.; Miljkovic, N., Lubricant-Infused Surfaces for Low-Surface-Tension Fluids: The Extent of Lubricant Miscibility. ACS Applied Materials & Interfaces 2021, 13, 19, 23121-23133.

[22] Wang, F.; Xiao, S. B.; Zhuo, Y. Z.; Ding, W. W.; He, J. Y.; Zhang, Z. L., Liquid layer generators for excellent icephobicity at extremely low temperatures. Materials Horizons 2019, 6 (10), 2063-2072.

[23] Chernyy, S.; Järn, M.; Shimizu, K.; Swerin, A.; Pedersen, S. U.; Daasbjerg, K.; Makkonen, L.; Claesson, P.; Iruthayaraj, J., Superhydrophilic Polyelectrolyte Brush Layers with Imparted Anti-Icing Properties: Effect of Counter ions. ACS Applied Materials & Interfaces 2014, 6 (9), 6487-6496.

[24] Li, W.; Zhan, Y.; Yu, S., Applications of superhydrophobic coatings in anti-icing: Theory, mechanisms, impact factors, challenges and perspectives. Progress in Organic Coatings 2021, 152, 106117.

[25] Irajizad, P.; Nazifi, S.; Ghasemi, H., Icephobic surfaces: Definition and figures of merit. Advances in Colloid and Interface Science 2019, 269, 203-218.

[26] Hejazi, V.; Sobolev, K.; Nosonovsky, M., From superhydrophobicity to icephobicity: forces and interaction analysis. Scientific Reports 2013, 3, 2194.

[27] Kreder, M. J.; Alvarenga, J.; Kim, P.; Aizenberg, J., Design of anti-icing surfaces: smooth, textured or slippery? Nature Reviews Materials 2016, 1 (1), 15003.

[28] Zhuo, Y.; Xiao, S.; Håkonsen, V.; He, J.; Zhang, Z., Anti-icing Ionogel Surfaces: Inhibiting Ice Nucleation, Growth, and Adhesion. ACS Materials Letters 2020, 2 (6), 616-623.

[29] Chen, J.; Dou, R.; Cui, D.; Zhang, Q.; Zhang, Y.; Xu, F.; Zhou, X.; Wang, J.; Song, Y.; Jiang, L., Robust Prototypical Anti-icing Coatings with a Self-lubricating Liquid Water Layer between Ice and Substrate. ACS Applied Materials & Interfaces 2013, 5 (10), 4026-4030.

[30] Chen, J.; Luo, Z.; Fan, Q.; Lv, J.; Wang, J., Anti-Ice Coating Inspired by Ice

Skating. Small 2014, 10 (22), 4693-4699.

[31] Qi, C.; Chen, H.; Shen, L.; Li, X.; Fu, Q.; Zhang, Y.; Sun, Y.; Liu, Y., Superhydrophobic Surface Based on Assembly of Nanoparticles for Application in Anti-Icing under Ultralow Temperature. ACS Applied Nano Materials 2020, 3 (2), 2047-2057.

[32] Kim, Y. G.; Lim, N.; Kim, J.; Kim, C.; Lee, J.; Kwon, K.-H., Study on the surface energy characteristics of polydimethylsiloxane (PDMS) films modified by C4F8/O_2/Ar plasma treatment. Applied Surface Science 2019, 477, 198-203.

[33] Li, Q.; Guo, Z. G., Fundamentals of icing and common strategies for designing biomimetic anti-icing surfaces. Journal of Materials Chemistry A 2018, 6 (28), 13549-13581.

[34] Cui, W.; Pakkanen, T. A., Fabrication of transparent icephobic surfaces with self-reparability: Effect of structuring and thickness of the lubricant-elastomer layer. Applied Surface Science 2020, 504, 144061.

[35] Li, H.; Li, X.; Luo, C.; Zhao, Y.; Yuan, X., Icephobicity of polydimethylsiloxane-b-poly(fluorinated acrylate). Thin Solid Films 2014, 573, 67-73.

[36] Arianpour, F.; Farzaneh, M.; Kulinich, S. A., Hydrophobic and ice-retarding properties of doped silicone rubber coatings. Applied Surface Science 2013, 265, 546-552.

[37] Li, X.; Zhao, Y.; Li, H.; Yuan, X., Preparation and icephobic properties of polymethyltrifluoropropylsiloxane–polyacrylate block copolymers. Applied Surface Science 2014, 316, 222-231.

[38] Jeon, J.; Jang, H.; Chang, J.; Lee, K.-S.; Kim, D. R., Fabrication of micro-patterned aluminum surfaces for low ice adhesion strength. Applied Surface Science 2018, 440, 643-650.

[39] Barthwal, S.; Lee, B.; Lim, S.-H., Fabrication of robust and durable slippery anti-icing coating on textured superhydrophobic aluminum surfaces with infused silicone oil. Applied Surface Science 2019, 496, 143677.

[40] Foroughi Mobarakeh, L.; Jafari, R.; Farzaneh, M., The ice repellency of plasma

polymerized hexamethyldisiloxane coating. Applied Surface Science 2013, 284, 459-463.

[41] Ling, E. J. Y.; Uong, V.; Renault-Crispo, J.-S.; Kietzig, A.-M.; Servio, P., Reducing Ice Adhesion on Nonsmooth Metallic Surfaces: Wettability and Topography Effects. ACS Applied Materials & Interfaces 2016, 8 (13), 8789-8800.

[42] Jamil, M. I.; Zhan, X.; Chen, F.; Cheng, D.; Zhang, Q., Durable and Scalable Candle Soot Icephobic Coating with Nucleation and Fracture Mechanism. ACS Applied Materials & Interfaces 2019, 11 (34), 31532-31542.

[43] Chen, D.; Gelenter, M. D.; Hong, M.; Cohen, R. E.; McKinley, G. H., Icephobic Surfaces Induced by Interfacial Nonfrozen Water. ACS Applied Materials & Interfaces 2017, 9 (4), 4202-4214.

[44] He, Z.; Zhuo, Y.; Wang, F.; He, J.; Zhang, Z., Design and preparation of icephobic PDMS-based coatings by introducing an aqueous lubricating layer and macro-crack initiators at the ice-substrate interface. Progress in Organic Coatings 2020, 147, 105737.

[45] Li, T.; Ibanez-Ibanez, P. F.; Hakonsen, V.; Wu, J.; Xu, K.; Zhuo, Y.; Luo, S.; He, J.; Zhang, Z., Self-Deicing Electrolyte Hydrogel Surfaces with Pa-level Ice Adhesion and Durable Antifreezing/Antifrost Performance. ACS Applied Materials & Interfaces 2020, 12 (31), 35572-35578.

[46] Tan, X.; Zhang, Y.; Liu, X.; Xi, S.; Yan, Z.; Liu, Z.; Shi, T.; Liao, G., Employing micro pyramidal holes and porous nanostructures for enhancing the durability of lubricant-infused surfaces in anti-icing. Surface & Coatings Technology 2021, 405, 126568.

[47] Donadei, V.; Koivuluoto, H.; Sarlin, E.; Vuoristo, P., Lubricated icephobic coatings prepared by flame spraying with hybrid feedstock injection. Surface & Coatings Technology 2020, 403, 126396.

[48] Aghdam, A. S.; Cebeci, F. C., Tailoring the Icephobic Performance of Slippery Liquid-Infused Porous Surfaces through the LbL Method. Langmuir 2020, 36 (46), 14145-14154.

[49] Zhao, L.; He, L.; Liang, J.; Chen, Y.; Jia, M.; Huang, J., Facile preparation of a

slippery oil-infused polymer surface for robust icephobicity. Progress in Organic Coatings 2020, 148, 105849.

[50]Li, T.; Zhuo, Y.; Hakonsen, V.; He, J.; Zhang, Z., Durable Low Ice Adhesion Foams Modulated by Submicrometer Pores. Industrial & Engineering Chemistry Research 2019, 58 (38), 17776-17783.

[51]Zhao, J.; Wang, Z.; Guo, P.; Luo, Q., Molecular level investigation of methane and carbon dioxide adsorption on SiO_2 surface. Computational Materials Science 2019, 168, 213-220.

[52] Jin, M.; Shen, Y.; Luo, X.; Tao, J.; Xie, Y.; Chen, H.; Wu, Y., A combination structure of microblock and nanohair fabricated by chemical etching for excellent water repellency and icephobicity. Applied Surface Science 2018, 455, 883-890.

[53] Zheng, S.; Bellido-Aguilar, D. A.; Wu, X.; Zhan, X.; Huang, Y.; Zeng, X.; Zhang, Q.; Chen, Z., Durable Waterborne Hydrophobic Bio-Epoxy Coating with Improved Anti-Icing and Self-Cleaning Performance. ACS Sustainable Chemistry & Engineering 2019, 7 (1), 641-649.

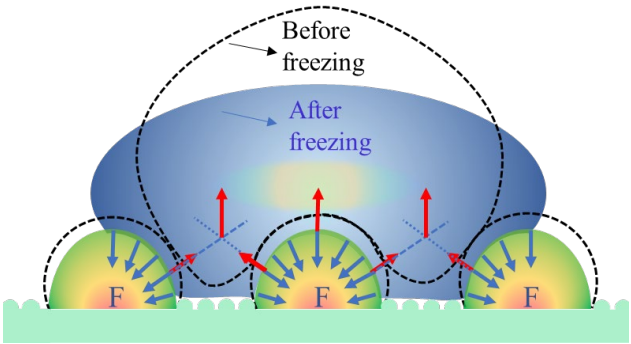

TOC 图